


# C9orf10/Ossa regulates the bone metastasis of established lung adenocarcinoma cell subline H322L-BO4 in a mouse model

Takamasa Uekita<sup>1</sup>  | Reiko Yagi<sup>2</sup> | Tohru Ichimura<sup>1</sup> | Ryuichi Sakai<sup>3</sup>

<sup>1</sup>Department of Applied Chemistry, National Defense Academy, Yokosuka, Japan

<sup>2</sup>Division of Metastasis and Invasion Signaling, National Cancer Center Research Institute, Tokyo, Japan

<sup>3</sup>Department of Biochemistry, Kitasato University School of Medicine, Kanagawa, Japan

## Correspondence

Takamasa Uekita, Department of Applied Chemistry, National Defense Academy, 1-10-20 Hashirimizu, Yokosuka 239-8686, Japan.

Email: [tuekita@nda.ac.jp](mailto:tuekita@nda.ac.jp)

## Funding information

JSPS KAKENHI, Grant/Award Number: JP21K07165

Communicated by: Kohei Miyazono

## Abstract

Lung cancer frequently metastasizes to the bones. An in vivo model is urgently required to identify potential therapeutic targets for the prevention and treatment of lung cancer with bone metastasis. We established a lung adenocarcinoma cell subline (H322L-BO4) that specifically showed metastasis to the leg bones and adrenal glands. This was achieved by repeated isolation of metastatic cells from the leg bones of mice. The cells were intracardially injected into nude mice. Survival was prolonged for mice that received H322L-BO4 cells versus original cells (H322L). H322L-BO4 cells did not exhibit obvious changes in general in vitro properties associated with the metastatic potential (e.g., cell growth, migration, and invasion) compared with H322L cells. However, the phosphorylation of chromosome 9 open reading frame 10/oxidative stress-associated Src activator (C9orf10/Ossa) was increased in H322L-BO4 cells. This result confirmed the increased anchorage independence through C9orf10/Ossa-mediated activation of Src family tyrosine kinase. Reduction of C9orf10/Ossa by shRNA reduced cells' metastasis to the leg bone and prolonged survival in mice. These findings indicate that H322L-BO4 cells can be used to evaluate the effect of candidate therapeutic targets against bone metastatic lung cancer cells. Moreover, C9orf10/Ossa may be a useful target for treatment of lung cancer with bone metastasis.

## KEYWORDS

anoikis resistance, bone metastasis, cancer metastasis, C9orf10/Ossa/FAM120A, lung adenocarcinoma, mouse model, signal transduction, Src family kinase

## 1 | INTRODUCTION

The skeletal system is one of the most frequent sites of metastases of nonsmall-cell lung cancer. Notably, 30%–40% of patients with advanced lung cancer develop bone

metastasis (Buijs & van der Pluijm, 2009; Coleman, 2001). Skeletal-related events (e.g., bone pain, spinal cord compression, and bone fracture) lead to poor quality of life. The recent development of novel therapies has improved the survival of patients with advanced lung

This is an open access article under the terms of the [Creative Commons Attribution-NonCommercial-NoDerivs](https://creativecommons.org/licenses/by-nc-nd/4.0/) License, which permits use and distribution in any medium, provided the original work is properly cited, the use is non-commercial and no modifications or adaptations are made.

© 2024 The Authors. *Genes to Cells* published by Molecular Biology Society of Japan and John Wiley & Sons Australia, Ltd.

cancer. However, there is a lack of effective therapeutic agents against bone metastasis. This is because the complex signals underlying the interaction between cancer cells and bone in the osseous microenvironment have not been elucidated (Coleman, 2001; Kingsley et al., 2007). It is thought that tumor cells exhibit metastatic organotropism, metastasize to specific target organs with characteristic preference, and acquire distinct organotropism-related molecules for adaptation to the different target organ microenvironments (Fidler, 2003; Kang et al., 2003). Although several studies have revealed the mechanisms of organ-specific metastasis to the bone microenvironment (Buijs & van der Pluijm, 2009; Holden & Raymond, 2003), it is unclear whether such distinct key regulators of organ-specific metastasis-related molecules exist. Therefore, we decided to establish bone metastatic lung cancer cell lines that could be used to explore and evaluate candidate molecules as therapeutic targets.

Tyrosine phosphorylation signals, including Src family tyrosine kinase (SFK) signals, are frequently upregulated in metastatic human cancer (Chang et al., 2008; Irby & Yeatman, 2000; Talamonti et al., 1993). Elevated SFK activity is thought to contribute to cancer development, progression, and metastasis (Brown & Cooper, 1996; Frame, 2002). Furthermore, in some cancerous cells, it is associated with osteoclast-mediated bone resorption, tumor growth, and bone metastasis (Roodman, 2004; Saad & Lipton, 2010). Accordingly, through the inhibition of both tumor and osteoclast activities, SFK may be effective in the treatment of advanced tumors accompanied by bone metastasis. Preclinical research showed that treatment with SFK inhibitors, such as dasatinib or saracatinib, suppresses the metastasis of prostate and breast cancer to the bones. Nevertheless, this treatment has been linked to side effects because SFK also plays an important role in normal cells (Saad & Lipton, 2010). Therefore, the elucidation and inhibition of cancer-specific SFK-mediated signaling may be effective in reducing the side effects caused by SFK inhibition.

Homo sapiens chromosome 9 open reading frame10 (C9orf10) was originally identified as an annotated protein in the human genome sequence project (Holden & Raymond, 2003). It regulates the activation of SFK in response to oxidative stress. Thus, C9orf10 is also termed oxidative stress of Src activator (Ossa). Recently, C9orf10/Ossa was also referred to as a family with sequence similarity 120 member A (FAM120A) (Bartolomé et al., 2015; Kelly et al., 2019). C9orf10/Ossa functions as an activator of SFK, unfolding its inactive form by association with both the SH2 and SH3 domains of SFK. In turn, tyrosine phosphorylation of C9orf10/Ossa is induced by the

activated SFK, producing scaffolds to recruit phosphatidylinositol 3-kinase (PI3K) and activate PI3K-Akt signaling. The latter plays a key role in protecting cancer cells from oxidative stress-induced apoptosis (Tanaka et al., 2009). It has been reported that C9orf10/Ossa plays an important role in scirrhous gastric carcinoma. However, its role in other types of cancer has not been reported thus far.

In this study, we established the H322L-BO4 cell line, a subline of the H322 lung adenocarcinoma cell line, which metastasizes specifically to the leg bones and adrenal glands of mice. Furthermore, we investigated if H322L-BO4 cells could be used to explore and/or assess therapeutic targets in a mouse model of bone metastasis.

## 2 | RESULTS

### 2.1 | Establishment and characterization of bone metastatic lung adenocarcinoma cell subline H322L-BO4

A noninvasive in vivo bioluminescent imaging system is a powerful tool for observing the formation and progression of metastatic cancer. We stably introduced the firefly luciferase gene into the H322 lung adenocarcinoma cell line (H322L). Expression of the firefly luciferase gene did not affect the morphology and tyrosine phosphorylation signals of H322L cells compared with parental H322 cells (Figure 1a,b). Initially, we intracardially injected H322L cells into BALB/c nude mice. The formation and expansion of the metastatic region of the cells were monitored using the IVIS<sup>®</sup> Imaging System (Xenogen/Caliper Life Sciences, Hopkinton, MA, USA). Metastases of H322L cells were detected 14 days after inoculation (Figure 1c), and dissection of the mice revealed the presence of metastatic foci mainly in the leg bones, brain, adrenal glands, ovaries, and stomach (Table 1: H322L). To establish a bone metastatic lung adenocarcinoma cell subline, we serially passaged H322L cells in nude mice through repeated intracardiac injection and performed ex vivo culture of tumor cells prepared from bone metastatic foci in the leg bone (Figure 1d,e). Thereafter, the H322L-BO4 cell line, which is an H322L cell subline after four in vivo inoculations, consistently metastasized specifically to the leg bones and adrenal glands (Table 1).

Next, we examined the functional differences between H322L and H322L-BO4 cells in vitro. There were no differences observed in the morphology, growth, migration, and invasion of H322L-BO4 cells compared with H322L cells (Figure 2a–c). However, H322L-BO4 cells exhibited a greater photon ratio in leg bones compared with H322L cells. This was examined through

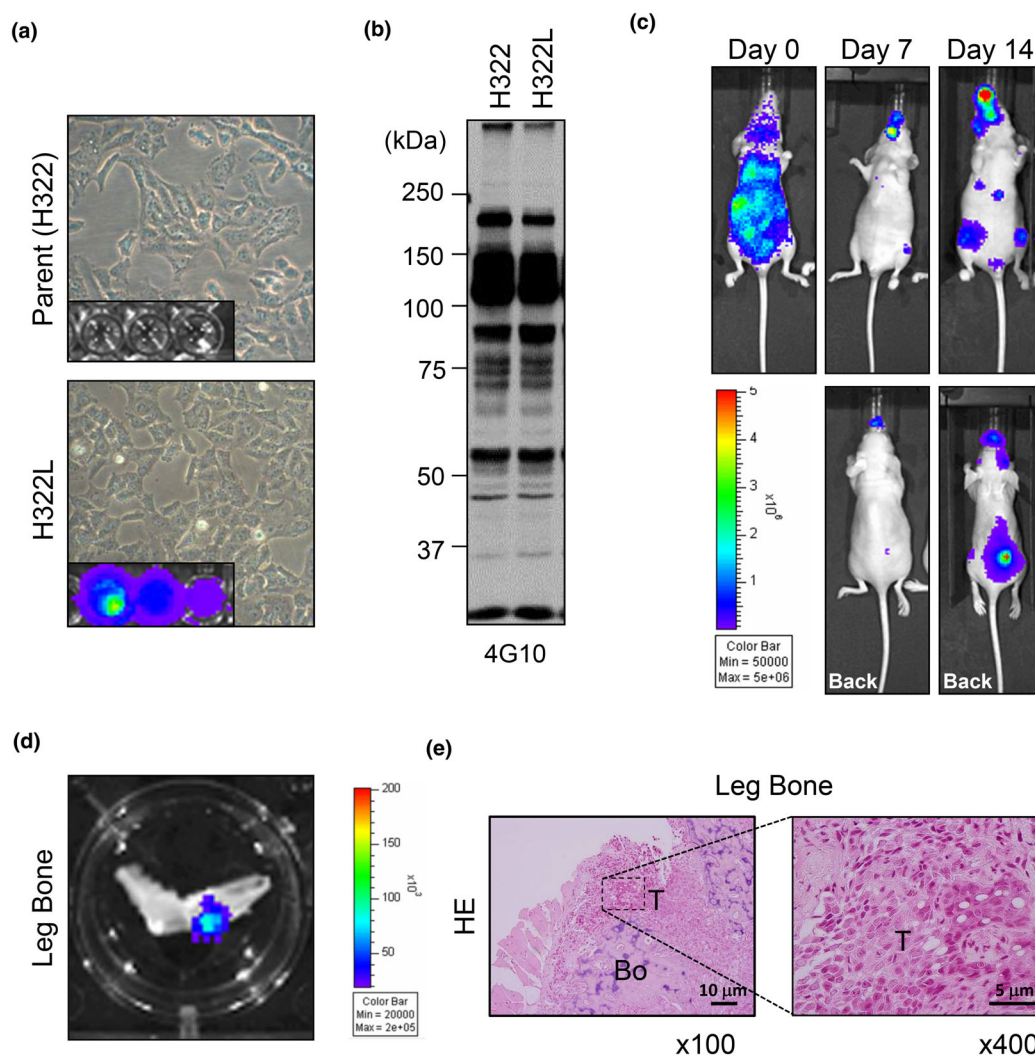


**FIGURE 1** Properties of H322L cells in preparation for establishing the H322L-BO4 cell subline. (a) Morphology of H322 cells and H322 cells with luciferase (H322L). (b) Western blotting using an anti-phosphotyrosine antibody in H322 and H322L cells. (c) Bioluminescent imaging of mice (abdomen side and back side) on 0, 7, and 14 days after intracardial injection of  $1 \times 10^6$  H322L cells. Back, backside. (d) Bioluminescent imaging detected metastatic H322L cells in the leg bones of mice. (e) Hematoxylin–eosin (H&E) staining of tissues obtained from the leg bones of mice (Magnification: 100 $\times$  and 400 $\times$ ). Bo, bone tissue; T, tumor tissue.

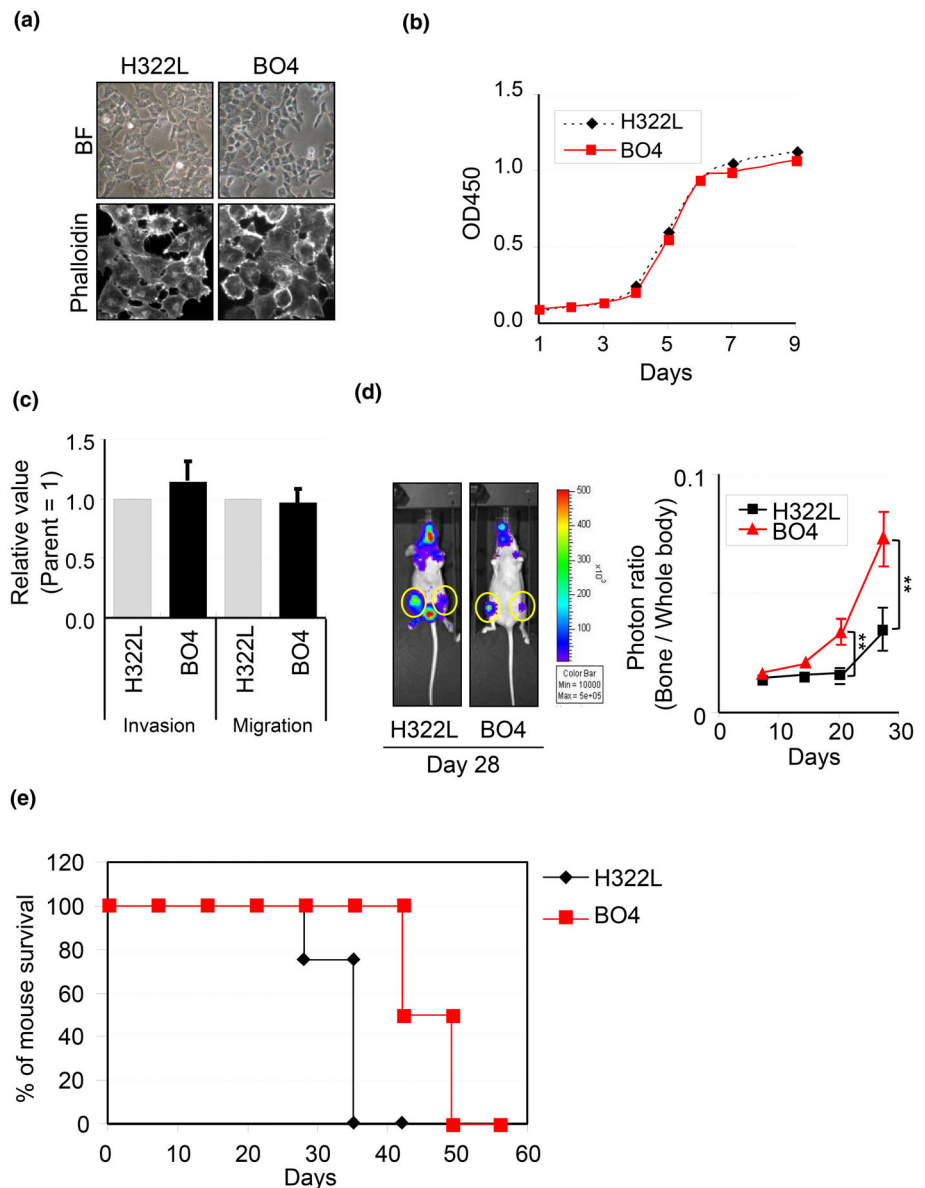
**TABLE 1** Establishment of the H322L cell subline (tissue specificity with repeated cardiac injections).

Metastatic region	H322L	H322L sublines					
		BO1	BO2	BO3	BO4	BO5	BO6
Limb bone (%)	8/8 (100)	3/3 (100)	3/3 (100)	3/3 (100)	6/6 (100)	2/2 (100)	2/2 (100)
Brain (%)	4/8 (50)	2/3 (67)	1/3 (33)				
Adrenal gland (%)	6/8 (75)	3/3 (100)	3/3 (100)	3/3 (100)	6/6 (100)	2/2 (100)	2/2 (100)
Ovary (%)	4/8 (50)	2/3 (67)	1/3 (33)	2/3 (67)			
Stomach (%)	3/8 (38)	1/3 (33)	1/3 (33)				
Intestine (%)		1/3 (33)					

injection of H322L-BO4 or H322L cells in nude mice and measurement of the photon levels of metastatic foci using the IVIS<sup>®</sup> imaging system (Figure 2d). Remarkably,

injection of H322L-BO4 cells prolonged survival compared with H322L cells (Figure 2e). These results indicate that the established cell subline H322L-BO4 may be a

**FIGURE 2** Comparison of the properties of H322L and H322L-BO4 cells. (a) Morphology of H322L cells and established H322L-BO4 cells. BF, bright field; Phalloidin, phalloidin staining. (b) Cell proliferation assay using Tetra Color One for H322L and H322L-BO4 cells. (c) Cell invasion and cell migration assay for H322L and H322L-BO4 cells. (d) Left panel, bioluminescent imaging of mice at 28 days after intracardial injection of  $1 \times 10^6$  H322L and H322L-BO4 cells in each mouse, Right panel, relative photon ratio at 7, 14, 21, and 28 days after intracardial injection of  $1 \times 10^6$  H322L and H322L-BO4 cells in each mouse on the abdomen side.  $**p < .05$ . (e) Survival rate of each mouse ( $n = 8$ ) after intracardial injection of  $1 \times 10^6$  H322L and H322L-BO4 cells.



useful tool for the production of bone metastatic mouse models of lung adenocarcinoma.

## 2.2 | C9orf10/Ossa regulates SFK activation and anchorage independence in H322L-BO4 cells

We examined the differences in tyrosine phosphorylation signals between H322L and H322L-BO4 cells using several antibodies. The results demonstrated that the phosphorylation of SFKs was increased in H322L-BO4 cells compared with H322L cells (Figure 3a: p-Src family [pY416]). Additionally, the phosphorylation of p130cas and C9orf10/Ossa (substrates of SFKs) increased in H322L-BO4 cells versus H322L cells (Figure 3a:

p-p130cas, IP:Ossa IB:4G10) and RT-PCR showed an increase in C9orf10/Ossa mRNA expression in H322L-BO4 cells compared with that in H322L cells (Figure S1). C9orf10/Ossa is an activator of SFKs in cells exposed to oxidative stress (Tanaka et al., 2009); therefore, we treated H322L-BO4 cells with hydrogen peroxide ( $H_2O_2$ ). Enhanced phosphorylation of SFKs was observed in H322L-BO4 cells treated with  $H_2O_2$  (Figure 3b), revealing that oxidative stress regulates SFK activation in H322L-BO4 cells.

Next, we attempted to suppress the levels of cancer-related molecules in H322L-BO4 cells using a plasmid shRNA system. Reduction of C9orf10/Ossa was confirmed by immunoblotting analysis (Figure 3c: Ossa #2, #4). SFK activation after treatment with  $H_2O_2$  was reduced in H322L-BO4 cells in which C9orf10/Ossa



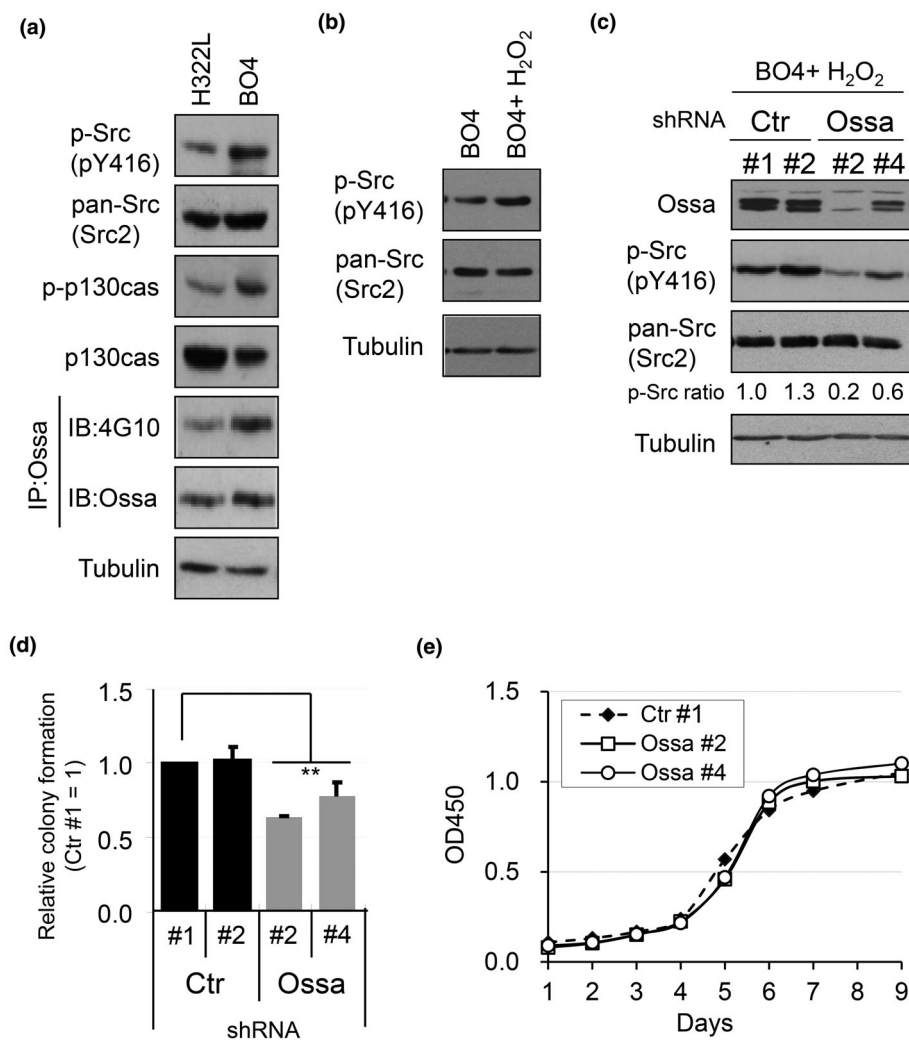


**FIGURE 3** Characterization of established H322L-BO4 cells.

(a) Western blotting for protein and phosphorylation of SFK, p130cas, and C9orf10/Ossa in H322L and H322L-BO4 cells. (b) Western blotting for activated SFK in H322L-BO4 cells before and after treatment with H<sub>2</sub>O<sub>2</sub>. (c) Western blotting comparing SFK activation in H322L-BO4 cells treated with shC9orf10/Ossa (Ossa#2, #4) and control shRNA (Ctr#1, #2). (d) Effects on anchorage independence using C9orf10/Ossa shRNA and soft agar assay in H322L-BO4 cells. \*\**p* < .05. (e) Effects on cell proliferation using C9orf10/Ossa shRNA detected by Tetra Color One in H322L-BO4 cells. C9orf10, chromosome 9 open reading frame 10; Ossa, oxidative stress-associated Src activator; SFK, Src family tyrosine kinase.

expression was stably reduced by shRNA (Ossa #2 and #4), compared with H322L-BO4 cells including the control shRNA (Ctr #1, #2) (Figure 3c). Additionally, we used H322L (Ossa+) cells, which transiently overexpressed C9orf10/Ossa protein (Figure S2A: Ossa+). Moreover, H322L (Mock) (Figure S2A: Mock), H322L-BO4 (Ctr#1), and H322L-BO4 (Ossa#2) cells were used to determine the ratio of apoptosis when cells were treated with H<sub>2</sub>O<sub>2</sub>. We observed a decreased apoptosis ratio in the H322L (Ossa+) cells compared with H322L (Mock) cells. In contrast, the apoptosis ratio increased in H322L-BO4 (Ossa#2) versus H322L-BO4 (Ctr #1) cells (Figure S2B). We observed reduction of anchorage independence in each shRNA-treated cell line compared with the control cells (Figure 3d) using a soft agar assay. In contrast, C9orf10/Ossa did not affect the growth of H322L-BO4 cells (Figure 3e). Moreover, we assessed anchorage independence through apoptosis of each cell line in suspension. Consistent with the soft agar assay results, H322L-BO4 (Ossa#2) cells displayed an increased apoptosis ratio compared with H322L-BO4 (Ctr#1) cells. However, H322L

(Ossa+) cells displayed a decreased apoptosis ratio compared with H322L (Mock) cells (Figure S3).

These results suggest that C9orf10/Ossa regulates the oxidative stress-induced apoptosis and anchorage independence of H322L-BO4 cells by activating SFKs.

### 2.3 | Effect of C9orf10/Ossa expression in a bone metastatic mouse model of lung cancer

We sought to examine whether the established H322L-BO4 cell line can be used as a model for investigating the effect of therapeutic candidate molecules. For this purpose, we used each C9orf10/Ossa-suppressed H322L-BO4 cell line (Ossa#2, #4). C9orf10/Ossa shRNA-expressing cells and control cells were intracardially injected into nude mice. Tumor formation and expansion were monitored weekly using the IVIS<sup>®</sup> system. In the metastatic mouse model, each Ossa-suppressed H322L-BO4 cell line (Ossa #2, #4) showed a trend toward a decrease in photon counts of the

whole mouse body compared with control H322L-BO4 cells (Ctr #1) (Figure 4a). The suppression ratio of *Ossa* expression by shRNA correlated with the ratio of reduction in photon counts of the whole mouse body (Figure 4a: *Ossa* #2, #4). The median survival time of mice that received H322L cells and H322L-BO4 cells was 32 and 36 days, respectively. These results indicated that injection of H322L-BO4 cells prolonged survival, as shown in Figure 2e. Furthermore, C9orf10/*Ossa* suppression further extended the median survival time of mice to 40 and 44 days, respectively (Figure 4b). This difference suggested a correlation with the rate of C9orf10/*Ossa* suppression.

These results indicate that C9orf10/*Ossa* is a candidate therapeutic target for bone metastatic lung cancer. In addition, this metastatic animal model using H322L-BO4 cells might be a useful system for evaluating therapeutic targets in bone metastatic lung cancer.

### 3 | DISCUSSION

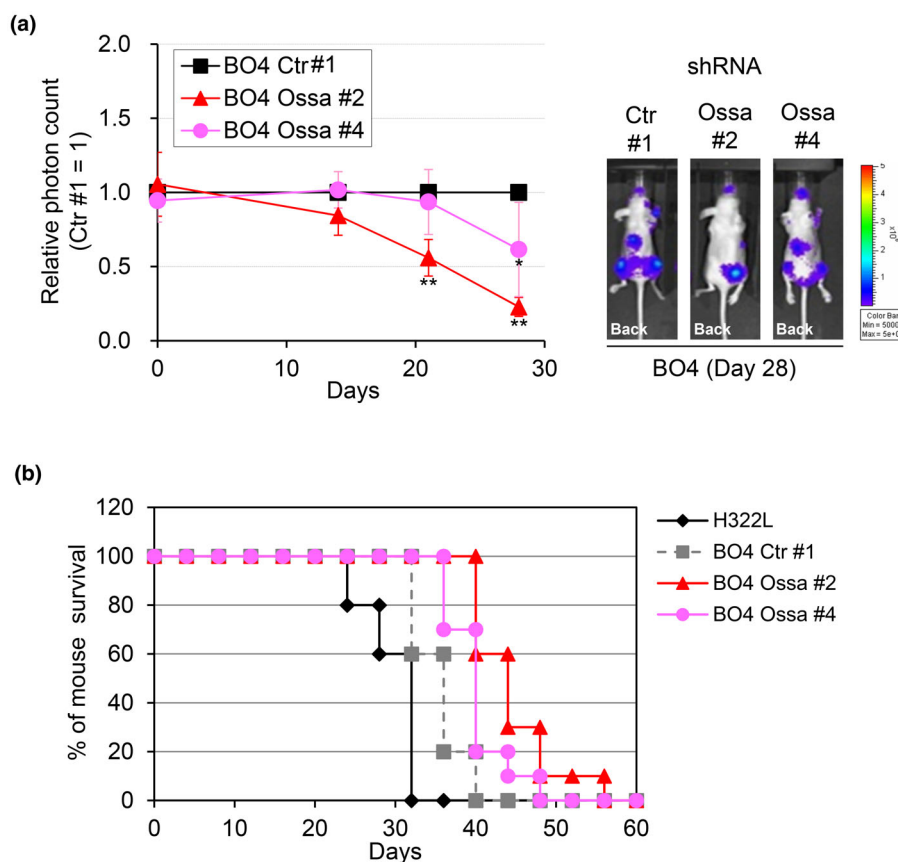
#### 3.1 | Establishment of bone metastatic mouse model using H322L-BO4 cells

In this study, we attempted to establish a cell line that could be used as an animal model of bone metastasis in a

noninvasive bioluminescence imaging system. We established H322L-BO4 cells, which did not show significant changes in their proliferative capacity, motility, or invasive capacity compared with H322L cells (Figure 2b,c). This evidence revealed that H322L-BO4 cells maintained the basic characteristics of H322L cells. Similar to other cancer cells, H322L cells metastasize to various organs in metastatic mouse models (Table 1), thereby causing debilitation early in mice. This effect complicates the study of the regulatory mechanisms of local metastasis to specific organs. However, the H322L-BO4 cells established in this study prolonged the survival period of mice after transplantation because of their improved tissue specificity for metastasis (Figure 2e). Therefore, we believe that the bone metastasis-related characteristics differed in H322L-BO4 cells compared with H322L cells. To address this concept, histological data would be required from the bone metastatic sites of H322L-BO4 and H322L cells. Overall, H322L-BO4 cells exhibited improved tissue specificity for metastasis, while maintaining the original cell characteristics. Thus, it is expected that the use of these cells will provide more detailed information on the mechanism underlying tissue-specific metastasis.

We tested the usefulness of the metastatic mouse model using H322L-BO4 cells. Initially, we used C9orf10/

**FIGURE 4** Effect of shC9orf10/*Ossa*-treated H322L-BO4 cells on a metastatic mouse model. (a) Left panel, ratio of photon counts of the whole mouse body in bioluminescence imaging at 14, 21, and 28 days after intracardiac injection of  $2 \times 10^6$  H322L-BO4 cells treated with control shRNA (Ctr #1) and C9orf10/*Ossa* shRNA (BO4 *Ossa* #2, #4). Right panel, bioluminescent imaging of the back side of mice at day 28 after intracardiac injection of  $1 \times 10^6$  H322L-BO4 cells treated with control shRNA (Ctr #1) and C9orf10/*Ossa* shRNA (BO4 *Ossa* #2, #4). Back, backside. \* $p < .1$ ; \*\* $p < .05$ . (b) Survival rate of each mouse ( $n = 10$ ) after intracardiac injection of  $2 \times 10^6$  H322L, control shRNA-treated H322L-BO4 cells (BO4 Ctr#1), and C9orf10/*Ossa* shRNA-treated H322L-BO4 cells (BO4 *Ossa* #2, #4). C9orf10, chromosome 9 open reading frame 10; *Ossa*, oxidative stress-associated Src activator; SFK, Src family tyrosine kinase.



Ossa because it activates SFK, thereby mediating bone metastasis in cancer cells (Tanaka et al., 2009). Moreover, C9orf10/Ossa phosphorylation was increased in H322L-BO4 cells compared with H322L cells (Figure 3a). A reduction in bone metastasis was observed in the mouse model following the suppression of C9orf10/Ossa expression in H322L-BO4 cells using the shRNA method (Figure 4a). In addition, the suppression of metastasis prolonged the survival of mice (Figure 4b). These results indicate that C9orf10/Ossa plays a role in regulating bone metastasis in metastatic mouse models. Furthermore, they suggest that H322L-BO4 could be a useful cell subline for understanding the mechanisms underlying bone metastasis of lung adenocarcinoma cells.

Bone metastatic cancer cells must survive and colonize bone tissue before complete formation of metastases. Herein, we demonstrated that C9orf10/Ossa is involved in survival (anchorage independence) rather than bone tissue colonization (organotropism). Since organotropism is an additionally important mechanism in bone metastasis, the organotropism-related factors of H322L-BO4 cells should thus be identified in the bone. For example, transforming growth factor- $\beta$  (TGF- $\beta$  signaling regulates osteoblastic metastasis in a prostate cancer mouse model (Mishra et al., 2011)), bone morphogenetic proteins (BMPs) and their signaling receptors are reportedly implicated in the development and progression of two distinct metastatic bone lesion types, osteoblastic and osteolytic lesions (Ye et al., 2011), and stimulator of interferon genes (STING) agonists protect against local bone destruction through osteoclast and immune cell function modulation in the tumor microenvironment (Wang et al., 2021). Further studies would be required to address if these factors could be involved in the bone metastasis of H322L-BO4 cells. Moreover, the established animal model can be used to monitor the formation and progression of tumor cells using noninvasive bioluminescent imaging with limited individual differences. We expect that this model will be a useful tool for the exploration and/or evaluation of therapeutic targets in lung cancer.

### 3.2 | Regulatory mechanisms of bone metastasis by C9orf10/Ossa in H322L-BO4 cells

Recently, it was reported that FAM120A (Ossa/C9orf10) is a putative RNA-binding protein, such as the novel argonaute RISC catalytic component 2 (Ago2) interacting protein (Bartolomé et al., 2015; Kelly et al., 2019). In addition, C9orf10/Ossa is one of the molecules that respond and transduce the downstream signaling pathway after stimulation of oxidative stress-associated cell

events (Tanaka et al., 2009). It has also been reported that C9orf10/Ossa is a substrate and activator of SFK (Tanaka et al., 2009). In H322L-BO4 cells established in this study, we observed activation of SFK under oxidative stress induced by H<sub>2</sub>O<sub>2</sub> (Figure 3b) and subsequent inhibition of SFK activity by C9orf10/Ossa inhibition (Figure 3c). This evidence indicates that C9orf10/Ossa is involved in SFK activation in H322L-BO4 cells. It has been shown that SFK activation plays an important role in cancer metastasis, including cell proliferation, cell motility, invasive ability, and anchorage independence (Sirvent et al., 2020). In this investigation, we found that C9orf10/Ossa regulates anchorage independence (Figure 3d). Anchorage independence is a property found only in cancer cells, allowing them to survive in a suspension state; moreover, it has been recognized as an important regulator of cancer metastasis (Wang et al., 2022). Recently, it was demonstrated that homophilic complex formation of the CUB domain-containing protein 1 (CDCP1), which regulates anchorage independence, is important for SFK activation in lung cancer cells (Sawayama et al., 2019). However, the original H322 cells remained anchorage-independent, although they expressed only low levels of CDCP1 (Uekita et al., 2007). Thus, C9orf10/Ossa regulates anchorage independence in H322L-BO4 cells as an SFK activator independently of CDCP1. In addition, the suppression of C9orf10/Ossa reduced the total amount of photons in the mouse body and did not affect site-specific metastasis to bone in terms of organ directivity (Figure 4a). These results indicate that C9orf10/Ossa may not be involved in the organotropism of H322L-BO4 cells during bone metastasis. Bone metastasis of lung cancer cells occurs due to their departure from the primary tumor and viability in the blood and bone microenvironment (Wu et al., 2021). It was recently reported that the tissue microenvironment is an important site where organotropism is promoted by tumor-derived extracellular vesicles (Rezaie et al., 2022). The bone microenvironment produces a hypoxic state; cancer cells can survive at low oxygen levels based on their distinctive signals (Annabi et al., 2003; Kingsley et al., 2007), while cancer cells in blood vessels must overcome oxidative stress. Therefore, C9orf10/Ossa may be involved in bone metastasis by regulating the anchorage independence of H322L-BO4 cells in the blood through signaling via SFK activation rather than organotropism. Bone metastasis is a common and serious complication of advanced malignancies, particularly concerning the three major malignancies (i.e., breast, prostate, and lung cancer). Therefore, the potential function of C9orf10/Ossa in breast and prostate cancer should also be investigated. In addition, because C9orf10/Ossa is involved in the regulation of SFK activity in lung cancer cells, it may be a useful target for the

discovery of novel agents from the perspective of SFK signaling inhibition. This is different from previous SFK inhibitors, such as dasatinib and saracatinib, used for the treatment of bone metastases.

## 4 | EXPERIMENTAL PROCEDURES

### 4.1 | Materials

The pan-Src antibody (Src2) was purchased from Santa Cruz Biotechnology (Santa Cruz, CA, USA). The phospho-Src family (pY416) antibody was purchased from Cell Signaling Technology (Beverly, MA, USA). The anti-phosphotyrosine (4G10) antibody was purchased from Upstate Biotechnology (Lake Placid, NY, USA). The  $\alpha$ -tubulin antibody was purchased from Sigma (St. Louis, MO, USA). The anti-C9orf10/Ossa, anti-p130cas, and anti-phospho-p130cas antibodies were prepared as previously described (Sakai et al., 1994; Tanaka et al., 2009). The sheep anti-mouse and sheep anti-rabbit antibodies were purchased from Cytiba (Tokyo, Japan). Alexa 594-conjugated phalloidin was obtained from Molecular Probes (Carlsbad, CA, USA).

### 4.2 | Cell culture and transfection of the firefly luciferase gene

H322 lung adenocarcinoma cells were maintained in RPMI 1640 medium supplemented with 10% fetal bovine serum (FBS; Equitech-Bio, Kerrville, TX, USA) at 37°C in a humidified atmosphere containing 5% CO<sub>2</sub>. G418 (500  $\mu$ g/mL; Sigma) was included to select cells expressing the firefly luciferase gene; puromycin (5  $\mu$ g/mL; Sigma) was also included to select shRNA-expressing cells. For luciferase gene transfection, H322 cells were seeded into a cell culture plate 24 h before transfection. The expression plasmid (pLucNeo) was kindly gifted by Dr. Ochiya (National Cancer Center Research Institute, Japan) (Kosaka et al., 2010). Transfection was performed with Lipofectamine 2000 according to the instructions provided by the manufacturer (Invitrogen, Carlsbad, CA, USA).

### 4.3 | Intracardiac injection and bioluminescent imaging

In vivo bioluminescent imaging was performed using the IVIS<sup>®</sup> Imaging System. Mice were anesthetized with isoflurane (Mylan Inc., Canonsburg, PA, USA) and received

$1 \times 10^6$  (in vivo passage, comparison of parental cells and BO4 cells) or  $2 \times 10^6$  (knockdown analyses) cells through intracardiac injection. At 10 min before imaging, the mice received D-Luciferin (Wako, Tokyo, Japan) at 150 mg/kg through intraperitoneal injection and images were captured under anesthesia with isoflurane. All images and measurements of bioluminescent signals were acquired and analyzed using the Living Image<sup>®</sup> software (Xenogen/Caliper Life Sciences). The in vivo experiments performed in this study were approved by the Committee for Ethics of Animal Experimentation and conducted in accordance with the Guidelines for Animal Experiments of the National Cancer Center Japan.

### 4.4 | Cell culture from a bone metastatic tumor

H322L cells were harvested from the culture plate and  $1 \times 10^6$  cells were intracardially injected into BALB/c nude mice (age: 4–6 weeks, female) purchased from CLEA Japan, Inc. (Japan). After 3 weeks, metastatic tissues were dissected from the hind limbs. Tissues were minced and treated with trypsin-ethylenediaminetetraacetic acid (trypsin-EDTA) solution supplemented with penicillin/streptomycin (Nacalai Tesque Inc., Kyoto, Japan) for 15 min at 37°C in a humidified atmosphere containing 5% CO<sub>2</sub>. Following trypsinization, cells were plated and incubated in RPMI 1640 medium containing 10% FBS, 500 ng/mL G418, 50  $\mu$ g/mL gentamicin, penicillin, and streptomycin.

### 4.5 | Retroviral shRNA infection

Target sequences of siRNA were designed using the target finder software ([http://www.ambion.com/techlib/misc/siRNA\\_finder.html](http://www.ambion.com/techlib/misc/siRNA_finder.html)). Retroviral shRNA plasmids were prepared using a pSilencer<sup>™</sup> 5.1-U6 kit (Ambion Inc., Austin, TX, USA) according to the instructions provided by the manufacturer. The target sequences used were: C9orf10/Ossa (#2) 5'-AAGTGATTGGTTTCTGCAGAG-3' and (#4) 5'-ACAAGATTGGCTGGGA-GAAG-3'. For retroviral production, Platinum-A cells were transfected with shRNA plasmids using Lipofectamine 2000 according to the instructions provided by the manufacturer. After 48 h, the retrovirus-containing medium was collected, centrifuged, and the supernatants were supplemented with H322L-BO4 cells. Western blotting was performed to confirm the molecular knockdown.



## 4.6 | Immunoprecipitation

Cell lysates were prepared with protease inhibitors in PLC buffer (10 mM Tris-HCl [pH 7.5], 5 mM ethylene glycol tetraacetic acid, 150 mM NaCl, 1% Triton X-100, 10% glycerol, 10 µg/mL aprotinin, 1 mM sodium orthovanadate [Na<sub>3</sub>VO<sub>4</sub>], and 100 µg/mL leupeptin). Protein concentration was measured using the BCA Protein Assay (Pierce). For purification, 5 µg of C9orf10/Ossa rabbit polyclonal antibody was added to the protein, which was subsequently incubated with 1 ml (2 mg/mL) of cell lysate for 2 h at 4°C. Next, the mixture was precipitated with Protein G Sepharose™ 4 Fast Flow (Cytiba, Tokyo, Japan) for 1 h at 4°C. The immunoprecipitates were extensively washed with PLC buffer and prepared for western blotting using the anti-phosphotyrosine (4G10) mouse monoclonal antibody.

## 4.7 | Western blotting

Whole-cell lysates prepared from H322L and H322L-BO4 cells were harvested using the PLC lysis buffer and used for immunoblotting. Equal amounts of total protein were separated by sodium dodecyl sulfate-polyacrylamide gel electrophoresis and transferred to polyvinylidene difluoride membranes. The membranes were incubated with primary antibodies overnight at 4°C and, subsequently, with horseradish peroxidase-conjugated secondary antibodies for 45 min at room temperature. Bands were detected on an x-ray film using an enhanced chemiluminescence system (Perkin Elmer, Waltham, MA, USA). Primary antibodies anti-pan-Src (Src2), anti-C9orf10/Ossa, anti-p130cas, and anti-phospho p130cas were used at 1:1000 dilution. Anti-phosphotyrosine (4G10), phospho-Src family (pY416), and  $\alpha$ -tubulin antibodies were used at 1:4000 dilution.

## 4.8 | Phalloidin staining

Cells cultured on coverslips were fixed with 4% paraformaldehyde for 10 min at room temperature. The samples were incubated with Alexa-594-conjugated phalloidin in the tris-buffered saline with Tween 20 buffer for 45 min at room temperature, and the coverslips were mounted on glass slides. The samples were examined using an Olympus IX-70 confocal laser scanning microscope. Phalloidin was used at 1:500 dilution.

## 4.9 | Cell growth assay

Cell growth was analyzed using Tetra Color One (Seikagaku, Tokyo, Japan) according to the instructions

provided by the manufacturer. In brief, cells were seeded in 96-well plates at  $3 \times 10^3$  cells/well. Following supplementation with Tetra Color One reagent, living cells were detected by measuring the absorbance at 450 nm wavelength with a microplate reader (iMark; Bio-Rad, Hercules, CA, USA). The experiment was performed in triplicate.

## 4.10 | Cell migration and cell invasion assays

Migration and invasion assays were performed using modified Transwell chambers with a polycarbonate nucleopore membrane (diameter: 6.5 mm; pore size: 8 µm) (Falcon™). Precoated filters (fibronectin 10 µg/mL, 100 µL) were dehydrated with 100 µL of medium and used for the invasion assay. Thereafter,  $5 \times 10^4$  cells in 100 µL of serum-free RPMI1640 were seeded into the upper compartment of each chamber, whereas the lower compartments were filled with 600 µL of the same medium supplemented with 10% FBS. Following incubation for 16 h in the cell migration assay or 24 h in the invasion assay at 37°C, nonmigrated cells on the upper surface of the filter were removed using a cotton swab, while the migrated cells on the lower surface of the filter were fixed and stained with Giemsa's Stain Solution (Azur-Eosin-Methylene Blue Solution; MUTO PURE CHEMICAL, Co.). The total number of migrated or invading cells was determined by counting cells in five microscopic fields per well at a magnification of  $\times 100$ . The extent of migration was expressed as the average number of cells per microscopic field. Cell migration and invasion assays were performed in triplicate.

## 4.11 | Soft agar assay

Six-well cell culture plates were coated with a layer of RPMI1640 supplemented with 10% FBS containing 0.5% UltraPure™ Agarose (Invitrogen). H322L-BO4 cells treated with or without C9orf10/Ossa shRNA clones were treated with trypsin/EDTA solution (Nacalai Tesque Inc.), washed twice in phosphate-buffered saline, and resuspended in RPMI1640 supplemented with 10% FBS at a density of  $6 \times 10^3$  cells/mL. Thereafter, a cell sample (500 µL) was added to 1 mL of RPMI1640 supplemented with 10% FBS containing 0.5% UltraPure™ Agarose (final 0.33%). The cells were plated onto the coated cell culture plates, the agar was allowed to solidify, and the plates were placed in a 37°C incubator. After 30 days, colonies formed in each

well were counted using a colony counter and the AMES software (version 1.00; Ieda Trading Co., Japan) for the comparison of anchorage independence. This experiment was performed in triplicate.

#### 4.12 | Statistical analysis

All data are presented as the mean  $\pm$  standard deviation. Tukey's test was used for multiple comparisons among sample groups.  $p < .1$  and  $p < .05$  indicate statistically significant differences.

#### ACKNOWLEDGMENTS

This work was supported by a Grant-in-Aid for Scientists from the Ministry of Education, Culture, Sports, Science and Technology of Japan (JSPS KAKENHI grant number: JP21K07165).

#### ORCID

Takamasa Uekita  <https://orcid.org/0000-0002-8491-7849>

#### REFERENCES

- Annabi, B., Lee, Y. T., Turcotte, S., Naud, E., Desrosiers, R. R., Champagne, M., Eliopoulos, N., Galipeau, J., & Béliveau, R. (2003). Hypoxia promotes murine bone-marrow-derived stromal cell migration and tube formation. *Stem Cells*, *21*, 337–347.
- Bartolomé, R. A., García-Palmero, I., Torres, S., López-Lucendo, M., Balyasnikova, I. V., & Casal, J. I. (2015). IL13 receptor  $\alpha 2$  signaling requires a scaffold protein, FAM120A, to activate the FAK and PI3K pathways in colon cancer metastasis. *Cancer Research*, *75*, 2434–2444.
- Brown, M. T., & Cooper, J. A. (1996). Regulation, substrates and functions of src. *Biochimica et Biophysica Acta*, *1287*, 121–149.
- Buijs, J. T., & van der Pluijm, G. (2009). Osteotropic cancers: From primary tumor to bone. *Cancer Letters*, *273*, 177–193.
- Chang, Y. M., Bai, L., Liu, S., Yang, J. C., Kung, H. J., & Evans, C. P. (2008). Src family kinase oncogenic potential and pathways in prostate cancer as revealed by AZD0530. *Oncogene*, *27*, 6365–6375.
- Coleman, R. E. (2001). Metastatic bone disease: Clinical features, pathophysiology and treatment strategies. *Cancer Treatment Reviews*, *27*, 165–176.
- Fidler, I. J. (2003). The pathogenesis of cancer metastasis: The 'seed and soil' hypothesis revisited. *Nature Reviews. Cancer*, *3*, 453–458.
- Frame, M. C. (2002). Src in cancer: Deregulation and consequences for cell behaviour. *Biochimica et Biophysica Acta*, *1602*, 114–130.
- Holden, S., & Raymond, F. L. (2003). The human gene Cxorfl7 encodes a member of a novel family of putative transmembrane proteins: cDNA cloning and characterization of Cxorfl7 and its mouse ortholog orf34. *Gene*, *318*, 149–161.
- Irby, R. B., & Yeatman, T. J. (2000). Role of Src expression and activation in human cancer. *Oncogene*, *19*, 5636–5642.
- Kang, Y., Siegel, P. M., Shu, W., Drobnjak, M., Kakonen, S. M., Cordon-Cardo, C., Guise, T. A., & Massagué, J. (2003). A multi-genic program mediating breast cancer metastasis to bone. *Cancer Cell*, *3*, 537–549.
- Kelly, T. J., Suzuki, H. I., Zamudio, J. R., Suzuki, M., & Sharp, P. A. (2019). Sequestration of microRNA-mediated target repression by the Ago2-associated RNA-binding protein FAM120A. *RNA*, *25*, 1291–1297.
- Kingsley, L. A., Fournier, P. G., Chirgwin, J. M., & Guise, T. A. (2007). Molecular biology of bone metastasis. *Molecular Cancer Therapeutics*, *6*, 2609–2617.
- Kosaka, N., Iguchi, H., Yoshioka, Y., Takeshita, F., Matsuki, Y., & Ochiya, T. (2010). Secretory mechanisms and intercellular transfer of microRNAs in living cells. *The Journal of Biological Chemistry*, *285*, 17442–17452.
- Mishra, S., Tang, Y., Wang, L., de Graffenried, L., Yeh, I. T., Werner, S., Troyer, D., Copland, J. A., & Sun, L. Z. (2011). Blockade of transforming growth factor-beta (TGFbeta) signaling inhibits osteoblastic tumorigenesis by a novel human prostate cancer cell line. *The Prostate*, *71*, 1441–1454.
- Rezaie, J., Ahmadi, M., Ravanbakhsh, R., Mojarad, B., Mahbubfam, S., Shaban, S. A., Shadi, K., Berenjabad, N. J., & Etemadi, T. (2022). Tumor-derived extracellular vesicles: The metastatic organotropism drivers. *Life Sciences*, *289*, 120216.
- Roodman, G. D. (2004). Mechanisms of bone metastasis. *The New England Journal of Medicine*, *350*, 1655–1664.
- Saad, F., & Lipton, A. (2010). SRC kinase inhibition: Targeting bone metastases and tumor growth in prostate and breast cancer. *Cancer Treatment Reviews*, *36*, 177–184.
- Sakai, R., Iwamatsu, A., Hirano, N., Ogawa, S., Tanaka, T., Mano, H., Yazaki, Y., & Hirai, H. (1994). A novel signaling molecule, p130, forms stable complexes in vivo with v-Crk and v-Src in a tyrosine phosphorylation-dependent manner. *The EMBO Journal*, *13*, 3748–3756.
- Sawayama, T., Nakashima, K., Ichimura, T., Sakai, R., & Uekita, T. (2019). Homophilic complex formation of CDCP1 via the extracellular CUB2 domain facilitates SFK activation and promotes cancer cell migration. *Oncology Reports*, *42*, 1507–1516.
- Sirvent, A., Mevizou, R., Naim, D., Lafitte, M., & Roche, S. (2020). Src family tyrosine kinases in intestinal homeostasis, regeneration and tumorigenesis. *Cancers*, *12*, 2014.
- Talamonti, M. S., Roh, M. S., Curley, S. A., & Gallick, G. E. (1993). Increase in activity and level of pp60c-src in progressive stages of human colorectal cancer. *The Journal of Clinical Investigation*, *91*, 53–60.
- Tanaka, M., Sasaki, K., Kamata, R., Hoshino, Y., Yanagihara, K., & Sakai, R. (2009). A novel RNA-binding protein, Ossa/C9orf10, regulates activity of Src kinases to protect cells from oxidative stress-induced apoptosis. *Molecular and Cellular Biology*, *29*, 402–413.
- Uekita, T., Jia, L., Narisawa-Saito, M., Yokota, J., Kiyono, T., & Sakai, R. (2007). CUB domain-containing protein 1 is a novel regulator of anoikis resistance in lung adenocarcinoma. *Molecular and Cellular Biology*, *27*, 7649–7660.
- Wang, J., Luo, Z., Lin, L., Sui, X., Yu, L., Xu, C., Zhang, R., Zhao, Z., Zhu, Q., An, B., Wang, Q., Chen, B.,

- Leung, E. L. H., & Wu, Q. (2022). Anoikis-associated lung cancer metastasis: Mechanisms and therapies. *Cancers (Basel)*, *14*, 4791.
- Wang, K., Donnelly, C. R., Jiang, C., Liao, Y., Luo, X., Tao, X., Bang, S., McGinnis, A., Lee, M., Hilton, M. J., & Ji, R.-R. (2021). STING suppresses bone cancer pain via immune and neuronal modulation. *Nature Communications*, *12*, 4558.
- Wu, S., Pan, Y., Mao, Y., Chen, Y., & He, Y. (2021). Current progress and mechanisms of bone metastasis in lung cancer: A narrative review. *Translational Lung Cancer Research*, *10*, 439–451.
- Ye, L., Mason, M. D., & Jiang, W. G. (2011). Bone morphogenetic protein and bone metastasis, implication and therapeutic potential. *Frontiers in Bioscience*, *16*, 865–897.

## SUPPORTING INFORMATION

Additional supporting information can be found online in the Supporting Information section at the end of this article.

**How to cite this article:** Uekita, T., Yagi, R., Ichimura, T., & Sakai, R. (2024). C9orf10/Ossa regulates the bone metastasis of established lung adenocarcinoma cell subline H322L-BO4 in a mouse model. *Genes to Cells*, *29*(4), 290–300. <https://doi.org/10.1111/gtc.13103>